Block magnetism coupled with local distortion in the iron-based spin-ladder compound $BaFe_2Se_3$

Yusuke Nambu,[1,2] Kenya Ohgushi,[2,3] Shunpei Suzuki,[3] Fei Du,[3,4] Maxim Avdeev,[5] Yoshiya Uwatoko,[2,3] Koji Munakata,[6] Hiroshi Fukazawa,[7] Songxue Chi,[8] Yutaka Ueda,[2,3] and Taku J. Sato[1,2]

[1]*Neutron Science Laboratory, Institute for Solid State Physics, University of Tokyo, 106-1 Shirakata, Tokai, Ibaraki 319-1106, Japan*

[2]*Japan Science and Technology Agency (JST), Transformative Research-Project on Iron Pnictides (TRIP), 5 Sanbancho, Chiyoda, Tokyo 102-0075, Japan*

[3]*Institute for Solid State Physics, University of Tokyo, Kashiwanoha, Kashiwa, Chiba 277-8581, Japan*

[4]*Key Laboratory of Advanced Batteries Physics and Technology, Ministry of Education, College of Physics, Jilin University, Changchun 130012, P.R. China*

[5]*Bragg Institute, Australian Nuclear Science and Technology Organisation, PMB1, Menai, NSW 2234, Australia*

[6]*Center for Neutron Science and Technology, Comprehensive Research Organization for Science and Society (CROSS), Tokai, Ibaraki 319-1106, Japan*

[7]*Quantum Beam Science Directorate, Japan Atomic Energy Agency, Tokai, Ibaraki 319-1195, Japan*

[8]*Neutron Sciences Directorate, Oak Ridge National Laboratory, Oak Ridge, TN 37831, USA*

(Received 29 December 2011; revised manuscript received 1 February 2012; published 22 February 2012)

Magnetism in the insulating $BaFe_2Se_3$ was examined through susceptibility, specific heat, resistivity, and neutron diffraction measurements. After formation of a short-range magnetic correlation, a long-range ordering was observed below $T_N \sim 255$ K. The transition is obscured by bulk properties. Magnetic moments ($\| a$) are arranged to form a Fe_4 ferromagnetic unit, and each Fe_4 stacks antiferromagnetically. This block magnetism is of the third type among magnetic structures of ferrous materials. The magnetic ordering drives unusually large distortion via magnetoelastic coupling.

DOI: 10.1103/PhysRevB.85.064413 PACS number(s): 75.25.−j, 72.20.−i, 75.30.Cr, 75.40.−s

I. INTRODUCTION

Since its discovery, iron-based superconductivity (SC) has become a main topic of research in condensed-matter physics.[1] The interplay between structure, magnetism, and SC is one of the most intriguing subjects of this field. The common theme is on the two-dimensional (2D) plane of iron, which has been realized in the ZrCuSiAs (1111), $ThCr_2Si_2$ (122), anti-PbO (11), and Cu_2Sb (111) structures. To gain further insight into the mechanism of SC, realization of, for example, different crystal and/or magnetic structures is desired. A recent prominent example is the 245 system,[2] in which a rare type of magnetic structure in an insulator has been discovered. Regarding crystal structure, achievement of SC over various dimensions is also ambitious. As spin ladders in copper oxides shed light on the mechanism of SC, a study on an analog with ladder geometry among ferrous compounds is highly interesting. Research on that compound can provide a unique opportunity to study electronic correlations and the importance of dimensionality for SC.

$BaFe_2Se_3$ is a realization of ladder geometry among iron-based compounds.[3] Unlike most parent compounds of the iron-based superconductors, $BaFe_2Se_3$ is an insulator down to the lowest measured temperature. The structure is unique, comprised of $FeSe_4$ tetrahedra with channels that host Ba atoms [Fig. 1(a)]. Four-fold coordinated Fe^{2+} ions extend along the b axis and form two-leg spin-ladder structure within the bc plane.

Here we report study of the iron-based spin-ladder compound $BaFe_2Se_3$ based on a high-quality polycrystalline sample. High-resolution powder neutron diffraction reveals a 3D magnetic order below $T_N \sim 255$ K. However, bulk properties such as magnetic susceptibility, electrical resistivity, and specific heat show no anomaly at the transition. Magnetic moments ($\sim$2.8 μ_B at 5 K) are arranged to form a Fe_4 ferromagnetic unit perpendicular to the ladder direction, and each Fe_4 stacks antiferromagnetically. This block magnetism, as in recently discovered 245 systems,[2] is the realization of the third type of magnetic structures among iron-based materials. Rietveld refinements on neutron diffraction data also reveal unusually large local lattice distortion driven by the magnetic order.

II. EXPERIMENTAL

High-quality polycrystalline $BaFe_2Se_3$ was grown by the solid-state reaction. We first synthesized the precursor $BaSe_3$. Stoichiometric amounts of elemental Ba shots and Se powder in an alumina crucible were sealed into an evacuated quartz ampoule that was slowly heated up to 700 °C, kept for 12 hrs, and then quenched to room temperature. The obtained $BaSe_3$ and Fe with a 1:2 molar ratio were mixed together and put into an alumina crucible inside a quartz tube. This was reacted at 700 °C for 96 hrs with an intermediate regrinding. The powder x-ray diffraction using Cu-K_α radiation indicates no trace of impurity phases, however, it turned out that there was a tiny amount of Fe_7Se_8 impurity by magnetization measurements. The electrical resistivity was measured by the standard four-probe method. The magnetic data were collected by using a superconducting quantum interference device (SQUID) magnetometer. The specific heat was measured by utilizing a commercial setup (Quantum Design, PPMS), where the relaxation method is used. Neutron powder diffraction data were collected on the high-resolution ECHIDNA diffractometer at the Australian Nuclear Science and Technology Organisation (ANSTO) and the Wide-Angle Neutron Diffractometer (WAND) at Oak Ridge National Laboratory (ORNL), with $\lambda = 2.4395$ and 1.4827 Å, respectively. Diffraction patterns were obtained between $T = 5$ and 350 K

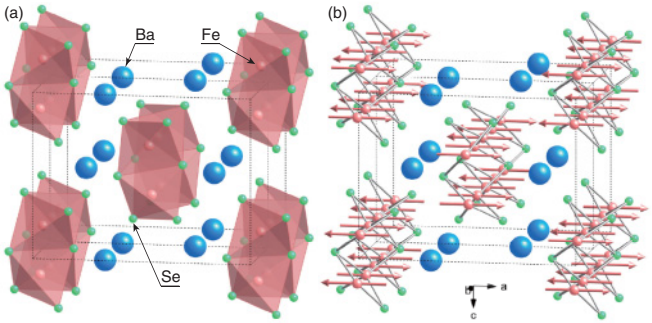

FIG. 1. (Color online) (a) Crystal and (b) magnetic structures of $BaFe_2Se_3$ at $T = 5$ K. Cuboids with dashed lines indicate crystallographic unit cells.

in a closed-cycle refrigerator. We employed group theoretical analysis to identify magnetic structures that are allowed by symmetry.

III. RESULTS AND DISCUSSION

Table I summarizes the structural parameters at $T = 300$ K determined by Rietveld refinement on powder neutron diffraction data. Consistent with other reports,[4–7] the crystal structure is accounted for by the orthorhombic space group *Pnma*. By keeping site occupancy variable for each of the atoms in the refinement, the result indicates the stoichiometric ratio within error bars, $Ba_{0.96(4)}Fe_{2.01(2)}Se_{3.02(7)}$. Temperature dependencies of lattice parameters are provided in Fig. 2(a), showing systematic change throughout the temperature regime.

Electrical resistivity ρ shows an insulating behavior [Fig. 2(b)]. Note that ρ exhibits no anomaly in the whole temperature range measured. A fitting with an activation-type formula $\rho = A\exp(\Delta/T)$ yields a small activation energy $\Delta = 0.13$ eV, comparable with Ref. 7. More precisely, ρ deviates from the activation-type behavior; instead it shows a variable-range-hopping-type (VRH) behavior. The data is fit to $\rho \propto \exp(B + (\frac{D}{T})^{\frac{1}{1+d}})$, where d denotes the dimension of the VRH model. The VRH in the 1D model yields better fit rather than the higher dimensions [inset to Fig. 2(b)]. This indicates that the compound is classified as a Mott-Anderson insulator, and is in the vicinity of metal-insulator (MI) transition. To further examine the conduction behavior, measurements on a single crystal are now underway.

Accurate magnetization measurement under a small applied field is limited by a tiny amount of ferromagnetic impurity,

TABLE I. Atomic positions within *Pnma* of $BaFe_2Se_3$ at $T = 300$ K determined by Rietveld analysis ($\chi^2 = 2.3$). Lattice constants are $a = 11.93178(15)$ Å, $b = 5.43747(6)$ Å, and $c = 9.16476(12)$ Å. Isotropic Debye-Waller factor (U_{iso}) is employed.

Atom	Site	x	y	z	U_{iso} (Å^2)
Ba	4*c*	0.1862(5)	1/4	0.5154(10)	0.051(5)
Fe	8*d*	0.4941(3)	0.0000(6)	0.3525(3)	0.044(2)
Se1	4*c*	0.3595(4)	1/4	0.2300(5)	0.059(5)
Se2	4*c*	0.6283(3)	1/4	0.4923(6)	0.034(4)
Se3	4*c*	0.3997(4)	1/4	0.8155(5)	0.061(5)

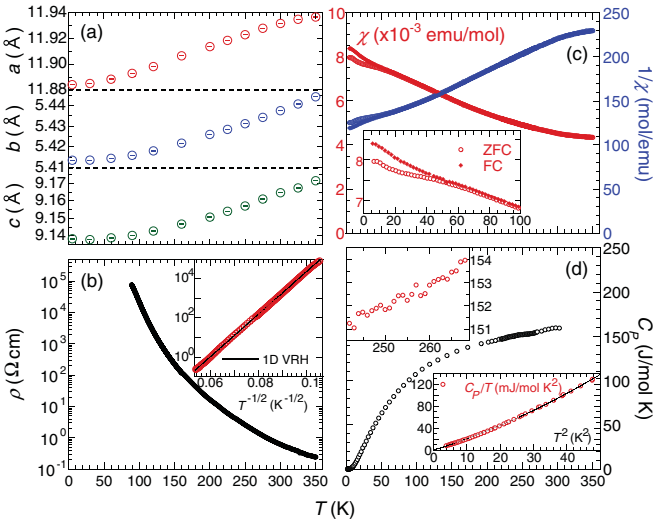

FIG. 2. (Color online) Temperature dependencies of (a) lattice parameters, (b) electrical resistivity (ρ), (c) magnetic susceptibility (χ) and its inverse, and (d) specific heat (C_P). The insets of (b),(c), and (d) show a fit with the 1D variable-range-hopping model (see text), enlargement of bifurcation, anomaly around T_N (left top), and C_P/T against T^2 with a polynomial fit (right bottom), respectively.

Fe_7Se_8 ($T_C \sim 460$ K).[8] We therefore deduce the susceptibility $\chi \equiv M/H$ under $\mu_0 H = 5$ T and subtract the one at 1 T to minimize effects from Fe_7Se_8. The key issue regarding the susceptibility is that it shows a weak temperature variation in the paramagnetic phase (above T_N) and does not obey the simple Curie-Weiss law [Fig. 2(c)]. One possible explanation for this is that a simple localized spin picture in a Mott-Anderson insulating state is invalid in the present system, which is close to the MI transition as anticipated by the small charge gap. Another possibility could be that the unquenched orbital angular momentum is present in Fe^{2+} ions owing to the prominence of the spin-orbit coupling in an orbital degenerated state. In contrast to the earlier report[5] indicating an emergence of weak ferromagnetism below T_N, our high-field susceptibility data show no prominent anomaly over the whole temperature range. This possibility is also excluded by our powder neutron data. As the inset to Fig. 2(c) shows, χ in zero-field-cooled (ZFC) and field-cooled (FC) sequences show small hysteresis. This could reflect glassy behavior caused by small randomness, but the origin of it is still unclear. From the data of ρ [Fig. 2(b)] and χ [Fig. 2(c)], we exclude the possibility of SC behavior of this compound, distinguished from Ref. 4.

Specific heat C_P shows no anomaly in the whole temperature measured [Fig. 2(d)]. Given no peak formation at around T_N [left-top inset to Fig. 2(d)], entropy release associated with the magnetic ordering turned out to be surprisingly small. A possible reason for this is that entropy release gradually occurs in a wide temperature range due to large fluctuations characterized in a low-dimensional system as will be discussed later. C_P/T versus T^2 plot at low temperatures indicates a negligible small T-linear contribution, as well as a small deviation from $C_P \propto T^3$ behavior [right-bottom inset to Fig. 2(d)]. The lack of γT term is in agreement with the Mott insulating nature, and inadequate fit with only βT^3 implies an existence of soft phonons. The data can be well reproduced by

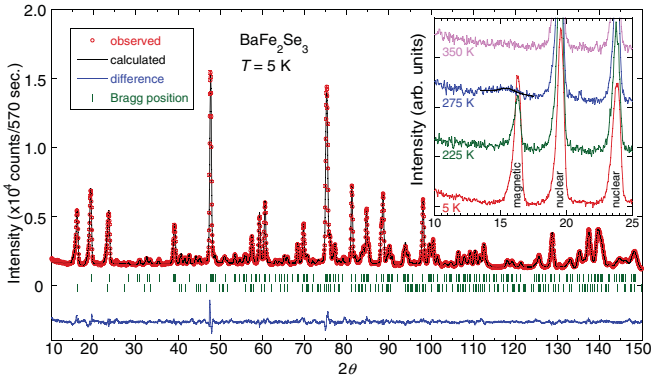

FIG. 3. (Color online) High-resolution neutron powder diffraction pattern of $BaFe_2Se_3$ at 5 K obtained on ECHIDNA with Rietveld refinement (solid lines). The calculated positions of nuclear and magnetic reflections are indicated (green ticks). The bottom line gives the difference between observed and calculated intensities. The inset shows temperature evolution of a magnetic reflection with short- (with black curve fit) and long-range correlations.

a function $C_P = \beta T^3 + \delta T^5$ with $\beta = 1.89$ mJ/mol K^4 and $\delta = 0.017$ mJ/mol K^6. If it is assumed that all the components of the β term come from the phonon contribution, using the formula $\beta = 12\pi^4 NR/5\theta_D^3$ (N being the number of atoms in a formula unit, 6), the Debye temperature (θ_D) is estimated to be 183 K. This value is considerably small and further supports the existence of soft phonons.

To gain microscopic information of magnetism, we performed high-resolution powder neutron diffraction. The obtained data is well fit based only on $BaFe_2Se_3$, and Fe_7Se_8 impurity has so small a volume fraction ($\lesssim 0.3\%$) that the secondary phase is not taken into account in the refinements. Additional resolution-limited peaks associated with magnetic ordering were observed below 250 K data. Figure 3 shows a diffraction pattern taken at 5 K along with the Rietveld refinement. To identify the magnetic structure, we applied representation analysis. All the magnetic peak positions can be accounted for by a propagation wave vector, (1/2,1/2,1/2). Basis vectors (BVs) of the irreducible representations (irreps) for the wave vector (Table II) were obtained using the SARA h code.[9] There are 24 BVs in total, belonging to two distinct irreps Γ_1 and Γ_2. Each irrep has 12 BVs, in which only four of eight Fe atoms in a unit cell are allowed to possess magnetic moments, and every BV describes the relation of moment direction of two atoms either parallel or antiparallel along one crystallographic axis. Both irreps in this case are required to participate as a corepresentation to let all eight atoms have magnetic moments. In a certain moment direction along either the a, b, or c axis, there are two choices for four combinations, namely 16 patterns. We assumed that the moment is parallel or antiparallel to one axis and has the same coefficient of four BVs, and sort out all 48 patterns to determine the magnetic structure by comparing R factors. The best fit with $R_{mag} = 8.54\%$ is a combination of BVs, ψ_4, ψ_{10}, ψ_{16}, and ψ_{22}, which is consistent with Ref. 5. The estimated moment at 5 K is 2.75(2) μ_B per an Fe^{2+} site. The 5 K magnetic structure corresponding to the best fit is shown in Fig. 1(b). Magnetic moments ($\| a$) are arranged to form a Fe_4 ferromagnetic unit in the bc plane, and each Fe_4 stacks antiferromagnetically (AF). For interladder coupling on the ac plane, block spins are AF correlated in one neighboring ladder and ferromagnetically (FM) correlated in the perpendicular direction. The next-nearest-neighbor ladders interact antiferromagnetically. The determined magnetic structure, described as block magnetism, is reminiscent of one observed in insulating $A_2Fe_4Se_5$ (A = K, Rb, Cs, Tl)[2] with a vacancy-ordered 2D Fe plane.

TABLE II. Basis vectors (BVs) of irreducible representations (irreps) for the space group $Pnma$ with the magnetic wave vector $\boldsymbol{q}_m = (1/2,1/2,1/2)$. Superscripts show the moment direction. Columns for positions represent #1: (x,y,z), #2: $(x+1/2, -y+3/2, -z+1/2)$, #3: $(-x+1, y-1/2, -z+1)$, #4: $(-x+1/2, -y+1, z+1/2)$, #5: $(-x+1, -y+1, -z+1)$, #6: $(-x+1/2, y-1/2, z+1/2)$, #7: $(x, -y+3/2, z)$, and #8: $(x+1/2, y, -z+1/2)$.

irrep	BV	#1	#2	#3	#4	#5	#6	#7	#8
Γ_1	ψ_1	2^a	0	0	0	0	0	-2^a	0
	ψ_2	2^b	0	0	0	0	0	2^b	0
	ψ_3	2^c	0	0	0	0	0	-2^c	0
	ψ_4	0	0	0	2^a	0	2^a	0	0
	ψ_5	0	0	0	2^b	0	-2^b	0	0
	ψ_6	0	0	0	-2^c	0	-2^c	0	0
	ψ_7	0	0	0	-2^a	0	2^a	0	0
	ψ_8	0	0	0	-2^b	0	-2^b	0	0
	ψ_9	0	0	0	2^c	0	-2^c	0	0
	ψ_{10}	2^a	0	0	0	0	0	2^a	0
	ψ_{11}	2^b	0	0	0	0	0	-2^b	0
	ψ_{12}	2^c	0	0	0	0	0	2^c	0
Γ_2	ψ_{13}	0	-2^a	0	0	0	0	0	-2^a
	ψ_{14}	0	2^b	0	0	0	0	0	-2^b
	ψ_{15}	0	2^c	0	0	0	0	0	2^c
	ψ_{16}	0	0	2^a	0	-2^a	0	0	0
	ψ_{17}	0	0	-2^b	0	-2^b	0	0	0
	ψ_{18}	0	0	2^c	0	-2^c	0	0	0
	ψ_{19}	0	0	2^a	0	2^a	0	0	0
	ψ_{20}	0	0	-2^b	0	2^b	0	0	0
	ψ_{21}	0	0	2^c	0	2^c	0	0	0
	ψ_{22}	0	2^a	0	0	0	0	0	-2^a
	ψ_{23}	0	-2^b	0	0	0	0	0	-2^b
	ψ_{24}	0	-2^c	0	0	0	0	0	2^c

Despite diverse structural and physical properties, there have been only several types of magnetic structures reported among iron-based materials. The common theme of magnetism and SC is on a square lattice of Fe with either pnictogen or chalcogen. In cuprates SC, parent compounds as Mott insulators show a simple AF pattern, a so-called checkerboard magnetic structure. This is favored by strong AF nearest-neighbor (nn) interactions, yet has not been observed in any ferrous compounds. The most common spin structure among the ferrous compounds is single-stripe magnetic structure. This features AF nn spins in one direction and ferromagnetically correlated in the perpendicular direction. Stripes extend along nn bonds as favored by next-nn AF exchange interactions. The single-stripe structure is observed in the parent compounds of the 1111, 122, and 111 materials. The double-stripe structure is also widely observed in the 11 systems[10] and insulating $La_2O_2Fe_2OSe_2$,[11] in which stripes extending again along nn

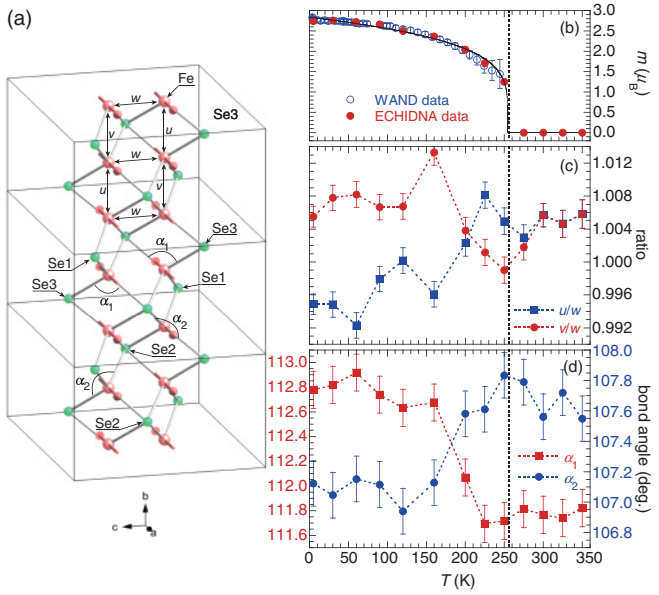

FIG. 4. (Color online) (a) A ladder geometry in $BaFe_2Se_3$. Solid lines surround unit cells. Temperature dependence of (b) estimated magnetic moment of the LRO, (c) ratio between lengths along the ladder (u,v) and leg (w) directions, and (d) representative angles (α_1,α_2) of Se-Fe-Se.

bonds in a structure that is favored by AF third nn interactions. The magnet $CaFe_4As_3$ with similar FeAs strips but connected in three dimensions has an incommensurate variant of the nearly double-stripe structure.[12,13] Finally, block magnetism has been recognized since the discovery of the 245 systems, in which nn Fe_4 atoms connected FM and the Fe plane is occupied by that block interacting AF with a separation of Fe vacancy. Note that this structure has magnetic moments perpendicular to the Fe plane, whereas the other structures have within-plane moments. There is a close relation between the magnetic structure and moment size; single-stripe structure typically has $\lesssim 1\ \mu_B$, double-stripe structure $\gtrsim 2\ \mu_B$, and block magnetism around $3\ \mu_B$. This classification is also the case for $BaFe_2Se_3$, which has large ($\sim 2.8\ \mu_B$) magnetic moments perpendicular to the ladder plane, belonging to the block magnetism.

Temperature dependence of the determined magnetic moment is shown in Fig. 4(b). Together with ECHIDNA and WAND data, T_N is roughly estimated to be 254.6 ± 2.4 K by an order-parameter-type fit. However, the previous Mössbauer experiment[14] reports no anomaly at around T_N, and instead clarifies the appearance of magnetic hyperfine splitting below 100 K. This distinct behavior could originate from the different timescale of the experimental technique; a neutron typically has a 10^{-12} sec timescale, being faster than that of Mössbauer (10^{-7} sec). Such a gradual slowing down of spin fluctuations is sometimes observed in low-dimensional magnets. If entropy release between 100 K and T_N was sufficient, the obscurity of it at the long-range order (LRO) might not be contradicted. Moreover, we observed a broad magnetic peak above T_N at slightly off position ($Q \sim 0.68$ Å^{-1}) from 0.73 Å^{-1} of the LRO [inset to Fig. 3]. This diffusive peak with the estimated correlation length of 19(5) Å, could also reflect the low dimensionality of the material. Elucidation of spin dynamics and short-range correlations realized by $BaFe_2Se_3$ would be important.

Despite the systematic lattice shrinkage as temperature decreased [Fig. 2(a)], significant local lattice distortion driven by the magnetic order is observed. Figure 4(a) depicts one ladder, where the summation of lengths, $u + v$ is equivalent to the lattice constant b, and w is the width of the ladder. Above T_N, u/w and v/w are completely overlapping each other and take slightly off value from the exact ladder (1.000) as shown in Fig. 4(c). They start to deviate after the magnetic order occurs; v/w shows a small increasing or constant behavior, whereas u/w is surely decreasing on cooling. This is attributed to change of the y position of Fe. We note that the atomic displacement along the b axis of Fe below T_N is as large as approximately 0.01 Å, which exceeds 10^{-5} Å reported in ordinary materials.[15] This is in contrast to the 245 systems, which show a shrinkage to the center of Fe_4 direction as favored by nn ferromagnetic interactions.[16] The distortion in $BaFe_2Se_3$ is also evidenced by change of the Se-Fe-Se bond angles [Fig. 4(d)]. Even above T_N, an $FeSe_4$ tetrahedron is distorted, and the magnetic ordering enhances it by elongating the lattice along the c axis. This splits e orbitals and stabilizes x^2-y^2 against $3z^2$-r^2, where the direction of the z orbital is perpendicular to the ladder plane. $BaFe_2As_2$ shows also similar temperature evolution of As-Fe-As angles across tetragonal to orthorhombic structural transition.[17] However, the angle change in $BaFe_2As_2$ is half as large as in $BaFe_2Se_3$. Given these facts of significant inherent lattice distortion, the x^2-y^2 orbital becomes firmly stabilized below T_N. Again, no symmetry change occurs at all in the temperature range from 5–350 K in $BaFe_2Se_3$. The orthorhombic $BaFe_2Se_3$ undergoes such a strong change due to magnetoelastic coupling without breaking the high-temperature symmetry. Instead it gives rise to the unusually large atomic displacement of Fe within the unit cell, and it can be consistent with the soft-phonon mode inferred from the specific heat results. It has been reported that the orthorhombicity ratio in $BaFe_2As_2$ is up to 3×10^{-3}, and it is systematically suppressed by electron doping to finally reach to SC.[18] $BaFe_2Se_3$, on the other hand, has almost twice as large distortion. Since this type of distortion is not preferred by SC in iron-based materials, applying pressure and doping studies are now under way to accomplish SC.

IV. SUMMARY

In summary we have examined Fe magnetism in the spin-ladder geometry realized in $BaFe_2Se_3$. A magnetic short-range correlation is detected, followed by a 3D long-range ordering. The transition is, however, obscured by bulk properties measurements. The determined magnetic structure is so-called block magnetism, where $\| a$ moments are arranged to form a Fe_4 ferromagnetic unit, and each Fe_4 stacks antiferromagnetically. The magnetic ordering also drives unusually large lattice distortion, which SC in ferrous compounds does not prefer.

ACKNOWLEDGMENTS

We thank M. Isobe for technical assistance and K. Okazaki for discussion. The work was supported in part by Grant-in-Aids for Scientific Research (Grant No. 2340097) and the Japanese Society for Neutron Science.

[1]For a review, see, e.g., G. R. Stewart, Rev. Mod. Phys. **83**, 1589 (2011).
[2]F. Ye, S. Chi, W. Bao, X. F. Wang, J. J. Ying, X. H. Chen, H. D. Wang, C. H. Dong, and M. Fang, Phys. Rev. Lett. **107**, 137003 (2011).
[3]H. Y. Hong and H. Steinfink, J. Solid State Chem. **5**, 93 (1972).
[4]A. Krzton-Maziopa, E. Pomjakushina, V. Pomjakushin, D. Sheptyakov, D. Chernyshov, V. Svitlyk, and K. Conder, J. Phys. Condens. Matter **23**, 402201 (2011).
[5]J. M. Caron, J. R. Neilson, D. C. Miller, A. Llobet, and T. M. McQueen, Phys. Rev. B **84**, 180409(R) (2011).
[6]B. Saparov, S. Calder, B. Sipos, H. Cao, S. Chi, D. J. Singh, A. D. Christianson, M. D. Lumsden, and A. S. Sefat, Phys. Rev. B **84**, 245132 (2011).
[7]H. Lei, H. Ryu, A. I. Frenkel, and C. Petrovic, Phys. Rev. B **84**, 214511 (2011).
[8]A. Okazaki, J. Phys. Soc. Jpn. **16**, 1162 (1961).
[9]A. S. Wills, Physica B **276-278**, 680 (2000); program available from [http://www.ccp14.ac.uk].
[10]W. Bao, Y. Qiu, Q. Huang, M. A. Green, P. Zajdel, M. R. Fitzsimmons, M. Zhernenkov, S. Chang, M. Fang, B. Qian, E. K. Vehstedt, J. Yang, H. M. Pham, L. Spinu, and Z. Q. Mao, Phys. Rev. Lett. **102**, 247001 (2009).
[11]D. G. Free and J. S. O. Evans, Phys. Rev. B **81**, 214433 (2010).
[12]P. Manuel, L. C. Chapon, I. S. Todorov, D. Y. Chung, J.-P. Castellan, S. Rosenkranz, R. Osborn, P. Toledano, and M. G. Kanatzidis, Phys. Rev. B **81**, 184402 (2010).
[13]Y. Nambu, L. L. Zhao, E. Morosan, K. Kim, G. Kotliar, P. Zajdel, M. A. Green, W. Ratcliff, J. A. Rodriguez-Rivera, and C. Broholm, Phys. Rev. Lett. **106**, 037201 (2011).
[14]M. Reissner, W. Steiner, and H. Boller, Hyper. Int. C: Proc. **5**, 197 (2002).
[15]S. Lee, A. Pirogov, M. Kang, K.-H. Jang, M. Yonemura, T. Kamiyama, S.-W. Cheong, F. Gozzo, N. Shin, H. Kimura, Y. Noda, and J.-G. Park, Nature **451**, 805 (2008).
[16]W. Bao (private communication).
[17]M. Rotter, M. Tegel, D. Johrendt, I. Schellenberg, W. Hermes, and R. Pöttgen, Phys. Rev. B **78**, 020503(R) (2008).
[18]M. G. Kim, R.M. Fernandes, A. Kreyssig, J. W. Kim, A. Thaler, S. L. Bud'ko, P. C. Canfield, R. J. McQueeney, J. Schmalian, and A. I. Goldman, Phys. Rev. B **83**, 134522 (2011).